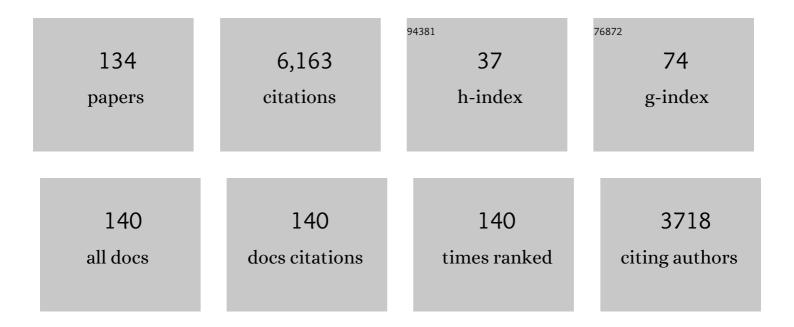
Pascal Spincemaille

List of Publications by Year in descending order

Source: https://exaly.com/author-pdf/6616613/publications.pdf Version: 2024-02-01



#	Article	IF	CITATIONS
1	Quantitative susceptibility map reconstruction from MR phase data using bayesian regularization: Validation and application to brain imaging. Magnetic Resonance in Medicine, 2010, 63, 194-206.	1.9	567
2	Morphology enabled dipole inversion for quantitative susceptibility mapping using structural consistency between the magnitude image and the susceptibility map. NeuroImage, 2012, 59, 2560-2568.	2.1	397
3	Calculation of susceptibility through multiple orientation sampling (COSMOS): A method for conditioning the inverse problem from measured magnetic field map to susceptibility source image in MRI. Magnetic Resonance in Medicine, 2009, 61, 196-204.	1.9	377
4	A novel background field removal method for MRI using projection onto dipole fields (PDF). NMR in Biomedicine, 2011, 24, 1129-1136.	1.6	352
5	Nonlinear formulation of the magnetic field to source relationship for robust quantitative susceptibility mapping. Magnetic Resonance in Medicine, 2013, 69, 467-476.	1.9	296
6	Morphology enabled dipole inversion (MEDI) from a singleâ€angle acquisition: Comparison with COSMOS in human brain imaging. Magnetic Resonance in Medicine, 2011, 66, 777-783.	1.9	290
7	Clinical quantitative susceptibility mapping (QSM): Biometal imaging and its emerging roles in patient care. Journal of Magnetic Resonance Imaging, 2017, 46, 951-971.	1.9	199
8	Nonlinear Regularization for Per Voxel Estimation of Magnetic Susceptibility Distributions From MRI Field Maps. IEEE Transactions on Medical Imaging, 2010, 29, 273-281.	5.4	192
9	Background field removal by solving the Laplacian boundary value problem. NMR in Biomedicine, 2014, 27, 312-319.	1.6	190
10	Cerebral Microbleeds: Burden Assessment by Using Quantitative Susceptibility Mapping. Radiology, 2012, 262, 269-278.	3.6	175
11	MEDI+0: Morphology enabled dipole inversion with automatic uniform cerebrospinal fluid zero reference for quantitative susceptibility mapping. Magnetic Resonance in Medicine, 2018, 79, 2795-2803.	1.9	132
12	Quantitative mapping of cerebral metabolic rate of oxygen (CMRO ₂) using quantitative susceptibility mapping (QSM). Magnetic Resonance in Medicine, 2015, 74, 945-952.	1.9	117
13	Reducing the object orientation dependence of susceptibility effects in gradient echo MRI through quantitative susceptibility mapping. Magnetic Resonance in Medicine, 2012, 68, 1563-1569.	1.9	110
14	Respiratory and cardiac selfâ€gated freeâ€breathing cardiac CINE imaging with multiecho 3D hybrid radial SSFP acquisition. Magnetic Resonance in Medicine, 2010, 63, 1230-1237.	1.9	109
15	Flow compensated quantitative susceptibility mapping for venous oxygenation imaging. Magnetic Resonance in Medicine, 2014, 72, 438-445.	1.9	104
16	Accuracy of the Morphology Enabled Dipole Inversion (MEDI) Algorithm for Quantitative Susceptibility Mapping in MRI. IEEE Transactions on Medical Imaging, 2012, 31, 816-824.	5.4	101
17	Reproducibility of quantitative susceptibility mapping in the brain at two field strengths from two vendors. Journal of Magnetic Resonance Imaging, 2015, 42, 1592-1600.	1.9	99
18	Preconditioned total field inversion (TFI) method for quantitative susceptibility mapping. Magnetic Resonance in Medicine, 2017, 78, 303-315.	1.9	99

#	Article	IF	CITATIONS
19	Age and sex related differences in subcortical brain iron concentrations among healthy adults. NeuroImage, 2015, 122, 385-398.	2.1	96
20	Simultaneous Phase Unwrapping and Removal of Chemical Shift (SPURS) Using Graph Cuts: Application in Quantitative Susceptibility Mapping. IEEE Transactions on Medical Imaging, 2015, 34, 531-540.	5.4	81
21	Magnetic susceptibility anisotropy: Cylindrical symmetry from macroscopically ordered anisotropic molecules and accuracy of MRI measurements using few orientations. NeuroImage, 2013, 70, 363-376.	2.1	75
22	<i>T</i> ₂ prep threeâ€dimensional spiral imaging with efficient whole brain coverage for myelin water quantification at 1.5 tesla. Magnetic Resonance in Medicine, 2012, 67, 614-621.	1.9	67
23	<i>In vivo</i> quantification of contrast agent concentration using the induced magnetic field for timeâ€resolved arterial input function measurement with MRI. Medical Physics, 2008, 35, 5328-5339.	1.6	66
24	3D texture analyses within the substantia nigra of Parkinson's disease patients on quantitative susceptibility maps and R2â^— maps. NeuroImage, 2019, 188, 465-472.	2.1	60
25	Bone quantitative susceptibility mapping using a chemical species–specific signal model with ultrashort and conventional echo data. Magnetic Resonance in Medicine, 2018, 79, 121-128.	1.9	58
26	Unambiguous identification of superparamagnetic iron oxide particles through quantitative susceptibility mapping of the nonlinear response to magnetic fields. Magnetic Resonance Imaging, 2010, 28, 1383-1389.	1.0	57
27	Cerebral metabolic rate of oxygen (CMRO ₂) mapping by combining quantitative susceptibility mapping (QSM) and quantitative blood oxygenation levelâ€dependent imaging (qBOLD). Magnetic Resonance in Medicine, 2018, 80, 1595-1604.	1.9	57
28	Joint estimation of chemical shift and quantitative susceptibility mapping (chemical QSM). Magnetic Resonance in Medicine, 2015, 73, 2100-2110.	1.9	53
29	Feasibility and reproducibility of whole brain myelin water mapping in 4 minutes using fast acquisition with spiral trajectory and adiabatic T2prep (FAST-T2) at 3T. Magnetic Resonance in Medicine, 2016, 76, 456-465.	1.9	53
30	Multiple sclerosis lesion geometry in quantitative susceptibility mapping (QSM) and phase imaging. Journal of Magnetic Resonance Imaging, 2015, 42, 224-229.	1.9	52
31	Effective motionâ€sensitizing magnetization preparation for black blood magnetic resonance imaging of the heart. Journal of Magnetic Resonance Imaging, 2008, 28, 1092-1100.	1.9	51
32	A fast navigatorâ€gated 3D sequence for delayed enhancement MRI of the myocardium: Comparison with breathhold 2D imaging. Journal of Magnetic Resonance Imaging, 2008, 27, 802-808.	1.9	49
33	Cerebral metabolic rate of oxygen (CMRO ₂) mapping with hyperventilation challenge using quantitative susceptibility mapping (QSM). Magnetic Resonance in Medicine, 2017, 77, 1762-1773.	1.9	47
34	Susceptibility underestimation in a highâ€susceptibility phantom: Dependence on imaging resolution, magnitude contrast, and other parameters. Magnetic Resonance in Medicine, 2017, 78, 1080-1086.	1.9	43
35	Fast 3D contrast enhanced MRI of the liver using temporal resolution acceleration with constrained evolution reconstruction. Magnetic Resonance in Medicine, 2013, 69, 370-381.	1.9	41
36	Noise Effects in Various Quantitative Susceptibility Mapping Methods. IEEE Transactions on Biomedical Engineering, 2013, 60, 3441-3448.	2.5	41

#	Article	IF	CITATIONS
37	Kalman filtering for realâ€ŧime navigator processing. Magnetic Resonance in Medicine, 2008, 60, 158-168.	1.9	39
38	Magnetic susceptibility increases as diamagnetic molecules breakdown: Myelin digestion during multiple sclerosis lesion formation contributes to increase on QSM. Journal of Magnetic Resonance Imaging, 2018, 48, 1281-1287.	1.9	34
39	Improved hepatic arterial phase MRI with 3â€second temporal resolution. Journal of Magnetic Resonance Imaging, 2013, 37, 1129-1136.	1.9	33
40	Quantitative Susceptibility Mapping of Time-Dependent Susceptibility Changes in Multiple Sclerosis Lesions. American Journal of Neuroradiology, 2019, 40, 987-993.	1.2	33
41	Quantitative susceptibility mappingâ€based cerebral metabolic rate of oxygen mapping with minimum local variance. Magnetic Resonance in Medicine, 2018, 79, 172-179.	1.9	32
42	Cluster analysis of time evolution (CAT) for quantitative susceptibility mapping (QSM) and quantitative blood oxygen levelâ€dependent magnitude (qBOLD)â€based oxygen extraction fraction (OEF) and cerebral metabolic rate of oxygen (CMRO ₂) mapping. Magnetic Resonance in Medicine, 2020, 83, 844-857.	1.9	32
43	Multicenter reproducibility of quantitative susceptibility mapping in a gadolinium phantom using MEDI+0 automatic zero referencing. Magnetic Resonance in Medicine, 2019, 81, 1229-1236.	1.9	31
44	Fidelity imposed network edit (FINE) for solving ill-posed image reconstruction. NeuroImage, 2020, 211, 116579.	2.1	31
45	An iterative spherical mean value method for background field removal in MRI. Magnetic Resonance in Medicine, 2014, 72, 1065-1071.	1.9	29
46	A New Advanced <scp>MRI</scp> Biomarker for Remyelinated Lesions in Multiple Sclerosis. Annals of Neurology, 2022, 92, 486-502.	2.8	28
47	Cardiac fat navigator-gated steady-state free precession 3D magnetic resonance angiography of coronary arteries. Magnetic Resonance in Medicine, 2006, 56, 210-215.	1.9	27
48	Threeâ€dimensional cine imaging using variableâ€density spiral trajectories and SSFP with application to coronary artery angiography. Magnetic Resonance in Medicine, 2007, 58, 535-543.	1.9	27
49	Z intensity-weighted position self-respiratory gating method for free-breathing 3D cardiac CINE imaging. Magnetic Resonance Imaging, 2011, 29, 861-868.	1.0	27
50	Rapid automated liver quantitative susceptibility mapping. Journal of Magnetic Resonance Imaging, 2019, 50, 725-732.	1.9	27
51	Quantitative Susceptibility Mapping: MRI at 7T versus 3T. Journal of Neuroimaging, 2020, 30, 65-75.	1.0	27
52	Direct coronary motion extraction from a 2D fat image navigator for prospectively gated coronary MR angiography. Magnetic Resonance in Medicine, 2014, 71, 599-607.	1.9	26
53	Quantification of cerebral perfusion using dynamic quantitative susceptibility mapping. Magnetic Resonance in Medicine, 2015, 73, 1540-1548.	1.9	25
54	Diagnostic accuracy of intracellular uptake rates calculated using dynamic Gdâ€EOBâ€DTPAâ€enhanced MRI for hepatic fibrosis stage. Journal of Magnetic Resonance Imaging, 2017, 45, 1177-1185.	1.9	25

#	Article	IF	CITATIONS
55	Deep neural network for water/fat separation: Supervised training, unsupervised training, and no training. Magnetic Resonance in Medicine, 2021, 85, 2263-2277.	1.9	24
56	Anticipatory Posturing of the Vocal Tract Reveals Dissociation of Speech Movement Plans from Linguistic Units. PLoS ONE, 2016, 11, e0146813.	1.1	24
57	Cardiac quantitative susceptibility mapping (QSM) for heart chamber oxygenation. Magnetic Resonance in Medicine, 2018, 79, 1545-1552.	1.9	23
58	Clinical Integration of Automated Processing for Brain Quantitative Susceptibility Mapping: Multi‣ite Reproducibility and Single‣ite Robustness. Journal of Neuroimaging, 2019, 29, 689-698.	1.0	22
59	Flip angle profile correction for <i>T</i> ₁ and <i>T</i> ₂ quantification with lookâ€locker inversion recovery 2D steadyâ€state free precession imaging. Magnetic Resonance in Medicine, 2012, 68, 1579-1585.	1.9	19
60	Validation of MRI quantitative susceptibility mapping of superparamagnetic iron oxide nanoparticles for hyperthermia applications in live subjects. Scientific Reports, 2020, 10, 1171.	1.6	18
61	View ordering for magnetization prepared steady state free precession acquisition: Application in contrast-enhanced MR angiography. Magnetic Resonance in Medicine, 2004, 52, 461-466.	1.9	16
62	Free-breathing 3-dimensional steady-state free precession coronary magnetic resonance angiography: comparison of four navigator gating techniques. Magnetic Resonance Imaging, 2009, 27, 807-814.	1.0	16
63	Initial Experience of Challenge-Free MRI-Based Oxygen Extraction Fraction Mapping of Ischemic Stroke at Various Stages: Comparison With Perfusion and Diffusion Mapping. Frontiers in Neuroscience, 2020, 14, 535441.	1.4	16
64	Quantitative Measurement of Metal Accumulation in Brain of Patients With Wilson's Disease. Movement Disorders, 2020, 35, 1787-1795.	2.2	15
65	Multiecho complex total field inversion method (mcTFI) for improved signal modeling in quantitative susceptibility mapping. Magnetic Resonance in Medicine, 2021, 86, 2165-2178.	1.9	15
66	DEEPMIR: a deep neural network for differential detection of cerebral microbleeds and iron deposits in MRI. Scientific Reports, 2021, 11, 14124.	1.6	15
67	Self-Gated Free-Breathing 3D Coronary CINE Imaging with Simultaneous Water and Fat Visualization. PLoS ONE, 2014, 9, e89315.	1.1	15
68	QSMRim-Net: Imbalance-aware learning for identification of chronic active multiple sclerosis lesions on quantitative susceptibility maps. NeuroImage: Clinical, 2022, 34, 102979.	1.4	15
69	Freeâ€breathing 3D steadyâ€state free precession coronary magnetic resonance angiography: Comparison of diaphragm and cardiac fat navigators. Journal of Magnetic Resonance Imaging, 2008, 28, 509-514.	1.9	14
70	Temporal clustering, tissue composition, and total variation for mapping oxygen extraction fraction using QSM and quantitative BOLD. Magnetic Resonance in Medicine, 2021, 86, 2635-2646.	1.9	14
71	How Accurate Is MOLLI T1 Mapping In Vivo? Validation by Spin Echo Methods. PLoS ONE, 2014, 9, e107327.	1.1	14
72	ALL-Net: Anatomical information lesion-wise loss function integrated into neural network for multiple sclerosis lesion segmentation. NeuroImage: Clinical, 2021, 32, 102854.	1.4	14

#	Article	IF	CITATIONS
73	Reduction of reconstruction time for time-resolved spiral 3D contrast-enhanced magnetic resonance angiography using parallel computing. Magnetic Resonance in Medicine, 2006, 56, 704-708.	1.9	13
74	Free breathing three-dimensional cardiac quantitative susceptibility mapping for differential cardiac chamber blood oxygenation – initial validation in patients with cardiovascular disease inclusive of direct comparison to invasive catheterization. Journal of Cardiovascular Magnetic Resonance, 2019, 21, 70.	1.6	13
75	Discontinuity Preserving Liver MR Registration With Three-Dimensional Active Contour Motion Segmentation. IEEE Transactions on Biomedical Engineering, 2019, 66, 1884-1897.	2.5	13
76	Brain oxygen extraction fraction mapping in patients with multiple sclerosis. Journal of Cerebral Blood Flow and Metabolism, 2022, 42, 338-348.	2.4	13
77	Effect of blood flow on double inversion recovery vessel wall MRI of the peripheral arteries: Quantitation with T 2 mapping and comparison with flow-insensitive T 2 -prepared inversion recovery imaging. Magnetic Resonance in Medicine, 2010, 63, 736-744.	1.9	12
78	Rapid whole brain myelin water content mapping without an external water standard at 1.5 T. Magnetic Resonance Imaging, 2017, 39, 82-88.	1.0	12
79	Quantitative susceptibility mapping of carotid plaques using nonlinear total field inversion: Initial experience in patients with significant carotid stenosis. Magnetic Resonance in Medicine, 2020, 84, 1501-1509.	1.9	12
80	Quantitative susceptibility mapping across two clinical field strengths: Contrastâ€ŧoâ€noise ratio enhancement at 1.5T. Journal of Magnetic Resonance Imaging, 2018, 48, 1410-1420.	1.9	11
81	Quantitative transport mapping (QTM) of the kidney with an approximate microvascular network. Magnetic Resonance in Medicine, 2021, 85, 2247-2262.	1.9	11
82	Cerebral oxygen extraction fraction: Comparison of dualâ€gas challenge calibrated BOLD with CBF and challengeâ€free gradient echo QSM+qBOLD. Magnetic Resonance in Medicine, 2021, 85, 953-961.	1.9	11
83	DCE-MRI quantitative transport mapping for noninvasively detecting hypoxia inducible factor-1α, epidermal growth factor receptor overexpression, and Ki-67 in nasopharyngeal carcinoma patients. Radiotherapy and Oncology, 2021, 164, 146-154.	0.3	11
84	QQâ€NET – using deep learning to solve quantitative susceptibility mapping and quantitative blood oxygen level dependent magnitude (QSM+qBOLD or QQ) based oxygen extraction fraction (OEF) mapping. Magnetic Resonance in Medicine, 2022, 87, 1583-1594.	1.9	11
85	Improved magnetization preparation for navigator steady-state free precession 3D coronary MR angiography. Magnetic Resonance in Medicine, 2004, 51, 1297-1300.	1.9	10
86	Quantitative susceptibility mapping of the spine using inâ€phase echoes to initialize inhomogeneous field and R2* for the nonconvex optimization problem of fatâ€water separation. NMR in Biomedicine, 2019, 32, e4156.	1.6	10
87	Clinical Integration of Quantitative Susceptibility Mapping Magnetic Resonance Imaging into Neurosurgical Practice. World Neurosurgery, 2019, 122, e10-e19.	0.7	10
88	A radial self alibrated (RASCAL) generalized autocalibrating partially parallel acquisition (GRAPPA) method using weight interpolation. NMR in Biomedicine, 2011, 24, 844-854.	1.6	9
89	On the influence of zero-padding on the nonlinear operations in Quantitative Susceptibility Mapping. Magnetic Resonance Imaging, 2017, 35, 154-159.	1.0	9
90	Clinical feasibility of brain quantitative susceptibility mapping. Magnetic Resonance Imaging, 2019, 60, 44-51.	1.0	9

#	Article	IF	CITATIONS
91	Susceptibility source separation from gradient echo data using magnitude decay modeling. Journal of Neuroimaging, 2022, 32, 852-859.	1.0	9
92	Free-Breathing 3D Imaging of Right Ventricular Structure and Function Using Respiratory and Cardiac Self-Gated Cine MRI. BioMed Research International, 2015, 2015, 1-9.	0.9	8
93	Increased risk for cerebral small vessel disease is associated with quantitative susceptibility mapping in HIV infected and uninfected individuals. NeuroImage: Clinical, 2021, 32, 102786.	1.4	8
94	Quantitative transport mapping (QTM) for differentiating benign and malignant breast lesion: Comparison with traditional kinetics modeling and semi-quantitative enhancement curve characteristics Magnetic Resonance Imaging, 2022, 86, 86-93.	1.0	8
95	BOLD New Directions in Myocardial Ischemia Imaging–Myocardial Oxygenation Assessment by Cardiac Magnetic Resonance. Journal of the American College of Cardiology, 2012, 59, 1965-1967.	1.2	7
96	Patch based reconstruction of undersampled data (PROUD) for high signal-to-noise ratio and high frame rate contrast enhanced liver imaging. Magnetic Resonance in Medicine, 2015, 74, 1587-1597.	1.9	7
97	Magnetic resonance microscopy may enable distinction between normal histomorphological features and prostate cancer in the resected prostate gland. BJU International, 2017, 119, 414-423.	1.3	7
98	Automated adaptive preconditioner for quantitative susceptibility mapping. Magnetic Resonance in Medicine, 2020, 83, 271-285.	1.9	7
99	Geometric Loss For Deep Multiple Sclerosis Lesion Segmentation. , 2021, , .		7
100	Quantitative Susceptibility Mapping for Staging Acute Cerebral Hemorrhages: Comparing the Conventional and <scp>Multiecho</scp> Complex Total Field Inversion magnetic resonance imaging <scp>MR</scp> Methods. Journal of Magnetic Resonance Imaging, 2021, 54, 1843-1854.	1.9	7
101	Global cerebrospinal fluid as a zeroâ€reference regularization for brain quantitative susceptibility mapping. Journal of Neuroimaging, 2022, 32, 141-147.	1.0	7
102	Contrast-Enhanced Magnetic Resonance Angiography with Biodegradable (Gd-DTPA)-Cystamine Copolymers:  Comparison with MS-325 in a Swine Model. Molecular Pharmaceutics, 2006, 3, 558-565.	2.3	6
103	Vastly accelerated linear leastâ€squares fitting with numerical optimization for dualâ€input delayâ€compensated quantitative liver perfusion mapping. Magnetic Resonance in Medicine, 2018, 79, 2415-2421.	1.9	6
104	Brain Iron Distribution after Multiple Doses of Ultra-small Superparamagnetic Iron Oxide Particles in Rats. Comparative Medicine, 2018, 68, 139-147.	0.4	6
105	The influence of molecular order and microstructure on the R2* and the magnetic susceptibility tensor. Magnetic Resonance Imaging, 2016, 34, 682-689.	1.0	5
106	Primalâ€dual and forward gradient implementation for quantitative susceptibility mapping. Magnetic Resonance in Medicine, 2017, 78, 2416-2427.	1.9	5
107	Sliding motion compensated low-rank plus sparse (SMC-LS) reconstruction for high spatiotemporal free-breathing liver 4D DCE-MRI. Magnetic Resonance Imaging, 2019, 58, 56-66.	1.0	5
108	Motion Artifact Suppression in Breath Hold 3D Contrast Enhanced Magnetic Resonance Angiography		4

using ECG Ordering. , 2006, 2006, 739-42.

#	Article	IF	CITATIONS
109	Threeâ€dimensional flowâ€independent balanced steadyâ€state free precession vessel wall MRI of the popliteal artery: Preliminary experience and comparison with flowâ€dependent blackâ€blood techniques. Journal of Magnetic Resonance Imaging, 2011, 34, 696-701.	1.9	4
110	A fast Edgeâ€preserving Bayesian reconstruction method for Parallel Imaging applications in cardiac MRI. Magnetic Resonance in Medicine, 2011, 65, 184-189.	1.9	4
111	Patents on Quantitative Susceptibility Mapping (QSM) of Tissue Magnetism. Recent Patents on Biotechnology, 2019, 13, 90-113.	0.4	4
112	Integrated quantitative susceptibility and R 2 * mapping for evaluation of liver fibrosis: An ex vivo feasibility study. NMR in Biomedicine, 2021, 34, e4412.	1.6	4
113	GAMER MRI: Gated-attention mechanism ranking of multi-contrast MRI in brain pathology. NeuroImage: Clinical, 2021, 29, 102522.	1.4	4
114	Highly accelerated 3D dynamic contrast enhanced MRI from sparse spiral sampling using integrated partial separability model and JSENSE. Proceedings of SPIE, 2014, , .	0.8	3
115	Brain Injury Lesion Imaging Using Preconditioned Quantitative Susceptibility Mapping without Skull Stripping. American Journal of Neuroradiology, 2018, 39, 648-653.	1.2	3
116	Temporal Feature Fusion with Sampling Pattern Optimization for Multi-echo Gradient Echo Acquisition and Image Reconstruction. Lecture Notes in Computer Science, 2021, , 232-242.	1.0	3
117	Subsecond accurate myelin water fraction reconstruction from FASTâ€T ₂ data with 3D UNET. Magnetic Resonance in Medicine, 2022, 87, 2979-2988.	1.9	3
118	Optimal coil array design: the two-coil case. Magnetic Resonance Imaging, 2007, 25, 671-677.	1.0	2
119	Reconstruction of highly under-sampled dynamic MRI using sparse representation of 1D temporal snippets. , 2015, , .		2
120	Quantitative evaluation of gadoxetate hepatocyte phase homogeneity: potential imaging markers for detection of early cirrhosis. Clinical Imaging, 2016, 40, 979-986.	0.8	2
121	Coherence enhancement in quantitative susceptibility mapping by means of anisotropic weighting in morphology enabled dipole inversion. Magnetic Resonance in Medicine, 2018, 79, 1172-1180.	1.9	2
122	Dipole modeling of multispectral signal for detecting metallic biopsy markers during MRIâ€guided breast biopsy: a pilot study. Magnetic Resonance in Medicine, 2020, 83, 1380-1389.	1.9	2
123	Spatially Adaptive Regularization in Total Field Inversion for Quantitative Susceptibility Mapping. IScience, 2020, 23, 101553.	1.9	2
124	Attenuation of motion artifacts in fMRI using discrete reconstruction of irregular fMRI trajectories (DRIFT). Magnetic Resonance in Medicine, 2021, 86, 1586-1599.	1.9	2
125	The central vein sign in multiple sclerosis lesions: Susceptibility relaxation optimization from a routine MRI multiecho gradient echo sequence. Journal of Neuroimaging, 2022, 32, 48-56.	1.0	1
126	The appearance of magnetic susceptibility objects in SWI phase depends on object size: Comparison with QSM and CT. Clinical Imaging, 2022, 82, 67-72.	0.8	1

#	Article	IF	CITATIONS
127	Noninvasive functional imaging of the heart using MRI: opportunities and challenges. , 2007, , .		0
128	Joint estimation of chemical shift and quantitative susceptibility mapping (chemical QSM). Magnetic Resonance in Medicine, 2015, 73, spcone-spcone.	1.9	0
129	A novel method for dipole inversion in QSM with reweighted L2-norm using distribution specification. , 2015, , .		0
130	Nonlinear profile order for three-dimensional hybrid radial acquisition applied to self-gated free-breathing cardiac cine MRI. Chinese Physics B, 2017, 26, 018701.	0.7	0
131	Quantitative Susceptibility Mapping of Magnetic Quadrupole Moments. Concepts in Magnetic Resonance Part A: Bridging Education and Research, 2019, 2019, 1-14.	0.2	0
132	Multispectral Imaging for Metallic Biopsy Marker Detection During MRI-Guided Breast Biopsy: A Feasibility Study for Clinical Translation. Frontiers in Oncology, 2021, 11, 605014.	1.3	0
133	Improved Signal-to-Noise Ratio in Parallel Coronary Artery Magnetic Resonance Angiography using Graph Cuts based Bayesian Reconstruction. Annual International Conference of the IEEE Engineering in Medicine and Biology Society, 2006, , .	0.5	Ο
134	Motion Artifact Suppression in Breath Hold 3D Contrast Enhanced Magnetic Resonance Angiography using ECG Ordering. Annual International Conference of the IEEE Engineering in Medicine and Biology Society, 2006, , .	0.5	0